Preprints.org

Article

Not peer-reviewed version

Injectable Hydrated Calcium Phosphate Bone-Like Paste: synthesis, In Vitro and In Vivo Biocompatibility Assessment

Anastasia Yu. Teterina *, Vladislav V. Minaychev, Polina V. Smirnova, Margarita I. Kobiakova, Igor V. Smirnov, Roman S. Fadeev, Alexey A. Egorov, Artem A. Ashmarin, Kira V. Pyatina, Anatoliy S. Senotov, Irina S. Fadeeva *, Vladimir S. Komlev *

Posted Date: 18 May 2023

doi: 10.20944/preprints202305.1261.v1

Keywords: biocompatible materials; calcium phosphates; hydrated pastes; bone tissue

Preprints.org is a free multidiscipline platform providing preprint service that is dedicated to making early versions of research outputs permanently available and citable. Preprints posted at Preprints.org appear in Web of Science, Crossref, Google Scholar, Scilit, Europe PMC.

Copyright: This is an open access article distributed under the Creative Commons Attribution License which permits unrestricted use, distribution, and reproduction in any medium, provided the original work is properly cited.

Preprints (www.preprints.org) | NOT PEER-REVIEWED | Posted: 18 May 2023 doi:10.20944/preprints202305.1261.v1

Disclaimer/Publisher's Note: The statements, opinions, and data contained in all publications are solely those of the individual author(s) and contributor(s) and not of MDPI and/or the editor(s). MDPI and/or the editor(s) disclaim responsibility for any injury to people or property resulting from any ideas, methods, instructions, or products referred to in the content.

Article

Injectable Hydrated Calcium Phosphate Bone-like Paste: Synthesis, *In Vitro* and *In Vivo* Biocompatibility Assessment

Anastasia Yu. Teterina [1], Vladislav V. Minaychev [1,2], Polina V. Smirnova [1], Margarita I. Kobiakova [1,2], Igor V. Smirnov [1], Roman S. Fadeev [2], Alexey A. Egorov [1], Artem A. Ashmarin [1], Anatoliy S. Senotov [2], Kira V. Pyatina [2], Irina S. Fadeeva [1,2,*] and Vladimir S. Komlev [1]

[1] A.A. Baikov Institute of Metallurgy and Materials Science, Russian Academy of Sciences, Leninskiy Prospect 49, Moscow 119334, Russia; teterina_imet@mail.ru (A.Yu.T.); baldyriz@gmail.com (I.V.S.);smirnova-imet@mail.ru (P.V.S.); komlev@mail.ru (V.S.K.)

[2] Institute of Theoretical and Experimental Biophysics, Russian Academy of Sciences, Pushchino 142290, Russia; aurin.fad@gmail.com (I.S.F.); vminaychev@gmail.com (V.V.M.); a.s.senotov@gmail.com (A.S.S.); fadeevrs@gmail.com (R.S.F.)

* Correspondence: aurin.fad@gmail.com (I.S.F.); teterina_imet@mail.ru (A.Y.T.); komlev@mail.ru (V.S.K.)

Abstract: The injectable hydrated calcium phosphate bone-like paste (hCPP) have been developed with suitable nanoscale characteristics and unindered injection through 23G standard needles. *In vitro* assays showed the cytocompatibility of hCPP with mesenchymal embryonic C3H10T1/2 cell cultures. The hCPP were identified to be composed of aggregated nano-sized particles with sphere-like shapes with low crystallinity. The ability of serum proteins (FBS) to adsorb on hCPP particles was also studied. The hCPP demonstrated high protein adsorption capacity, thereby indicating its potential in various biomedical applications. The results of the *in vivo* assay upon subcutaneous injection in Wistar rats indicated the nontoxicity and biocompatibility of experimental hCPP, as well as the gradual resorption of hCPP, comparable to the period of bone regeneration. The data obtained are of great interest for the development of commercial highly effective osteoplastic materials for bone tissue regeneration and augmentation.

Keywords: biocompatible materials; calcium phosphates; hydrated pastes; bone tissue

1. Introduction

The fabrication of injectable biocompatible, resorbable, osteoconductive, and bioactive bone-repairing pastes or gels is of great interest for the effective treatment of bone tissue defects [1–4]. Considering the present level of surgical technology and difficulties faced by traditional scaffolds, biocompatible and bioactive hydrated pastes or hydrogels remain the most promising substances for the regeneration of bone tissue. Injectable form provides a great advantage in orthopedic and dental surgery, as it can be minimally invasively delivered through a cannulated needle or catheter into the bone defect, and they can also enable a more uniform distribution of bioactive calcium phosphate molecules within internal space [5,6]. From a clinical point of view, such materials are very attractive as they can be used with minimal pain for the patient and maximum convenience for the surgeon, both for minimally invasive filling of the distance for consolidation of bone fragments or sinus lift surgery techniques and for optimal filling of irregularly shaped bone defects [7]. In addition, injectable pastes or gels for filling bone voids (fillers) are very popular and are used to fill bone voids in the skeletal system and provide the possibility of multiple minimally invasive additions of material without traumatic surgical manipulations, including long-term treatment after a vertebral fracture or resection of tumors and bone cysts.

Injectable bone materials may be cementitious or hydrogel based [10–13]. Acrylate bone cement has a variety of applications in orthopedic surgery (e.g., kyphoplasty and vertebroplasty), but it also has some shortcomings, such as high heat generation during polymerization and lack of integration

© 2023 by the author(s). Distributed under a Creative Commons CC BY license.

Preprints (www.preprints.org) | NOT PEER-REVIEWED | Posted: 18 May 2023 doi:10.20944/preprints202305.1261.v1

with bone tissue [14–16]. The exothermic reaction during cement hardening has an additional damaging effect on the surrounding bone tissue and impairs the regeneration processes [17,18]. Hydrogel-injectable materials have been developed as alternatives to cements. These hydrogel materials mainly consist of calcium phosphate powder evenly distributed in a polymer gel carrier. Calcium phosphates (CP) have been widely used as injectable form of bone graft for orthopedic surgery owing to their excellent properties in terms of biocompatibility and osteoconductivity [1,19]. Such injectable CP gels are prepared from powders and liquid components that form a paste that can be injected into a bone defect in situ upon mixing [9]. In modern practice, injectable CPs are synthesized using a combination of rapidly and slightly resorbable calcium phosphates, such as calcium sulfate and hydroxyapatite in a resorbable polymer gel [10,12,13,20].

Bone is considered to be a hierarchical biocomposite primarily composed of hydroxyapatite bio-ceramic, therefore, synthetic hydroxyapatite (HAp) have been used in medical applications because of its bio-inspired nature, lack of immunogenicity, relatively low cost of production and biological activity; HAp usually used as a slowly resorable base [21]. Calcium sulfate has a nonporous crystalline structure and structure-independent rate of incorporation, which is consistent in terms of dissolution/incorporation [10,11]. Calcium sulfate (CaS) is typically used as a rapidly resorbable bioactive agent and as a regenerative material to repair bone defects because it releases calcium ions into the surrounding microenvironment and promotes osteoblast differentiation [10,11]. Hydrogels are profoundly hydrated materials composed of three-dimensional hydrophilic polymeric systems comparable to those in normal tissues. The astuteness and rheological properties of hydrogels depend on the cross-linking between the polymer chains. Hydrogels have been broadly investigated as injectable materials because of their high tissue-like water content, ability to mimic the extracellular matrix, efficient mass transfer, amenability to chemical and physical modifications, and minimally invasive delivery [22]. Injectable hydrogel cements mainly incorporate polymers, such as alginate, chitin, chitosan, cellulose, gelatin, and collagen, and synthetic polymers, such as polyethylene glycol (PEG), poly (lactic-co-glycolic acid) (PLGA), polycaprolactone (PCL), and poly (L-lactic acid) (PLLA) [23–26]. However, most CaP-polymer systems have many disadvantages such as an increased inflammatory reaction, which may be explained by the well-known adjuvant and immunoactivating properties of these substances [27–31]. Consequently, the inflammatory process may be more pronounced in such materials, and the rate of material-associated bone tissue regeneration may be significantly higher than that in the empty control.

On the other hand, it is known that the most clinically effective pastes are based on the combination of nanosized HA with water. Clinical and animal data for the first gener-ation of nanoscale calcium phosphate paste products (including NANOSTIM (Med-tronic, USA) and ReproBone®novo (Ceramisys Ltd. Sheffield, UK)) are encouraging, suggesting that they are capable of promoting bone tissue regeneration [2,32]. The reasons for the good clinical performance may be the extremely high surface area-to-volume ratio, bioinspired use of nanoscale calcium phosphates, and hydration layer on the nanoparticle surfaces, which have a great influence on the subsequent protein adsorption and cell adhesion [33,34]. Considering the fact that CPs obtained by high-temperature synthesis do not have the necessary biological properties, and the body's response to them is limited to either the formation of a fibrous capsule around the material or the development of an inflammatory response [35–37].

We believe that injectable bone-repairing pastes must mimic the inorganic bone composition and have very specific hydrated surface kinetics to facilitate the migration, attachment, and proliferation of osteoprogenitor cells. Simultaneously, the calcium phosphate components used must be obtained under conditions as close as possible to physiological conditions, such as those occurring in native bone tissue.

Thus, the main goal of this study is to develop an approach for creating low-temperature injectable bone-like pastes, which are a combination of hydrated low-temperature hydroxyapatite with varying degrees of crystalline phase.

Preprints (www.preprints.org) | NOT PEER-REVIEWED | Posted: 18 May 2023 doi:10.20944/preprints202305.1261.v1

2. Materials and Methods

2.1. Synthesis Procedure and Characterization

2.1.1. Synthesis hCPP

The initial materials from Sigma ltd were used in the work except for the cases in-dicated separately in the text. Distilled water and ethyl alcohol rectified from food raw materials were used for synthesis and washing of filtration products.

The preparation of hydrated calcium phosphate paste (hCPP) samples by synthe-sis of nanopowders of HAp. Liquid-phase method of deposition from solutions allows to receive non-stoichiometric HAp with low degree of crystallization and various forms and with high specific surface area.

The hCPPs were prepared by stepwise mixing of ammonium phosphate salts with a concentration of 0.6 M, calcium nitrate with a concentration of 1 M under constant stirring with an overhead stirrer at 150 - 200 rpm. The pH value of the system in the range from 10.5 to 11.0 was maintained with an aqueous ammonia solution. The tem-perature of the reaction medium was 18 °C.

2.1.2. X-ray diffraction analysis

The phase composition of the obtained hCPPs were studied on a Shimadzu XRD-6000 diffractometer with an automated imaging system allowing data collection, graphical processing, and identification of the obtained phases from the JCPDS 2003 data bank. X-ray phase studies for general phase analysis were performed on powder dried samples under CuKα monochromatized radiation.

hCPPs were taken and subjected to drying in the thermostat at 37 °C for 24 h. Then the dried hCPP powders were rubbed through a sieve with a mesh size of 100 microns and transferred for analysis.

To confirm the reaction and the phase composition of the obtained powder a sample of the obtained hCPP was also additionally subjected to high-temperature treatment. For this purpose, a sample of 5 - 6 g was taken from the obtained hCPP samples, they were dried in a desiccator at 120 °C and then burned in a furnace with SiC heaters in an air atmosphere at 1250 °C for 2 h. The heating rate was 10 °C per minute.

2.1.3. Infrared spectroscopy

Infrared determination of absorption spectra of hCPP samples was carried out on a Nicolet Avatar 330 FT-IR spectrometer in the range of 7800-350 cm^{-1} with a resolution of 0.9 cm^{-1}. Samples of hCPP samples dried at 37 °C and hCPP powders after burning at 1250 °C were used for spectral analysis. For the study, samples of hCPP in powder form were mixed with potassium bromide. The spectra were analyzed based on reference and literature data.

2.1.4. Specific surface area hCPP

The specific surface area of calcium phosphate particles in the obtained hCPP was determined by BET low-temperature nitrogen adsorption on a Tristar 3000 Micromeritics instrument. The basis of the method is the measurement of the amount of substance required for the formation of an adsorption layer on the surface of a solid state. The determination is based on the number of molecules in the monolayer and the area occupied by each of them.

2.2. In vitro Studies

2.2.1. Cell Culture

Murine embryonic mesenchymal cell line C3H/10T1/2 was obtained from ATCC (Manassas, VA, USA). Cells were grown in Basal Medium Eagle (Sigma-Aldrich, Milwaukee, WI, USA) supplemented with heat-inactivated fetal bovine serum (Gibco, Waltham, MA, USA) to a final

Preprints (www.preprints.org) | NOT PEER-REVIEWED | Posted: 18 May 2023 doi:10.20944/preprints202305.1261.v1

concentration of 10% and 2 mM L-glutamine (Sigma-Aldrich, St. Louis, MO, USA), 40 μg/mL gentamicin sulfate (Sigma-Aldrich, St. Louis, MO, USA), under conditions of 5% CO_2 content in the air and at 37 °C. Cells of 7–10 passages were used in the experiments. The cell cultures were tested for mycoplasma infection using the MycoFluor™ Mycoplasma Detection Kit (Thermo Fisher Scientific, Waltham, MA, USA), and no mycoplasma was detected.

2.2.2. Cytotoxicity Assays

Murine embryonic mesenchymal cell line C3H/10T1/2 were seeded in amount of 5 × 103 cells in 100 μL of complete growth medium into 96-well plates (Corning Inc., Corning, NY, USA). After 24 h of cultivation, the medium was replaced with 100 μL of medium containing hCPP, at concentrations of 10, 3, 1, 0.3, and 0.1 mg/mL, and the cultivation was continued for 24 and 96 h. The cells in the control conditions were cultured in the medium without the addition of hCPP. hCPP was pre-sterilized with 75% ethanol according to the indicated method [38]. Then, cell viability was analyzed, as well as morphological analysis of the cell culture conditions.

The cytotoxicity of hCPP and the morphological state of the cell culture were analyzed by in vitro staining of cells with the fluorescent dyes Hoechst 33342 (stains blue nuclei of living and dead cells), propidium iodide (stains red nuclei of dead cells), and calcein AM (stains green cytoplasm of living cells). Cells were stained by adding 1 μg/mL Hoechst 33342 (Sigma-Aldrich, St. Louis, MO, USA), 1 μg/mL propidium iodide (Sigma-Aldrich, St. Louis, MO, USA), and 2 mM Calcein AM (Sigma-Aldrich, St. Louis, MO, USA) to the culture medium. The staining was performed in a CO_2 incubator for 30 min at 37 °C and 5% CO_2 in the air.

Microscopic analysis of the stained cell cultures and micro images was made on a Nikon Eclipse Ti-E (Nikon, Tokyo, Japan). The plate with cells and examined samples was transferred to a microscope chamber at 37°C and 5% CO_2 content. Cytotoxicity was analyzed by calculating the number of live and dead cells per field of view using the ImageJ software (https://imagej.nih.gov/ij/ (accessed on 19 April 2022)).

2.2.3. Protein Adsorption Assay

To determine the protein sorption capacity, hCPP were incubated in PBS with 10% FBS for 24 h. The final concentration of hCPP in the mixture was 10 mg/ml. PBS with 10% FBS was used as a control. The samples were incubated on an orbital shaker (S-3M A10, ELMI, Riga, Latvia) at room temperature with constant stirring at 21 rpm. To remove hCPP after incubation, the samples were subjected to centrifugation for 5 min at 5000 rpm using a Universal 320R centrifuge (Hettich, Westphalia, Germany). Protein concentration in the supernatant was determined using the Bradford method [39] at an absorption wavelength of 595 nm using an Imark plate reader (Bio-Rad, Hercules, California, USA).

2.3. In vivo Studies

2.3.1. Animals

Twenty Wistar male rats, weighing 190-200 g (age two months), were used. Animals were individually housed in a temperature-controlled room (22°C) and fed a standard diet, with full access to water and food. The experiments were carried out according to the Regulations for Studies with Experimental Animals (Decree of the Russian Ministry of Health of 12 August 1997, No. 755). The protocol was approved by the Commission on Biological Safety and Ethics at the Institute of Theoretical and Experimental Biophysics, Russian Academy of Sciences (March 2022, protocol N26/2022). For the experiments, rats were divided into four groups (five in each group) and independent replicates were done for each group.

2.3.2. Surgical Subcutaneous Injection

Preprints (www.preprints.org) | NOT PEER-REVIEWED | Posted: 18 May 2023 doi:10.20944/preprints202305.1261.v1

The model of ectopic (subcutaneous) implantation of biomaterials was used to study the biocompability of hCPP samples in vivo (ISO 10993-6). This model is advantageous and in addition to biocompatibility and safety analysis, it is used to evaluate the osteoinductive and osteogenic effects of substances [40,41]. Therefore, a heterotopic implantation model (under the skin, into the muscle, etc., but not into the bone) is the most reliable for revealing the osteoinductive and osteogenic potential of the materials under development.

The manipulations were performed under general anesthesia with Xylazine 13 mg/kg (Interchemie, The Netherlands) and Zoletil 7 mg/kg (Virbac, Carros, France). An aliquot of paste (500 ml) or saline solution was subcutaneously injected into the dorsal interscapular area of each group of animals. For post-surgical recovery, the animals were exposed to a heating plate until awakening. The animals from each group were randomly divided to be euthanized (carbon dioxide protocol) after 3, 8 or 13 weeks of the subcutaneous injection. Immediately after humane euthanasia, to prevent autolysis, instantly after the withdrawal samples of implanted materials, with surrounding tissues of the recipient bed, were washed for 30 s with a cold (14°C) isotonic solution, and fixed for 48 h in neutral buffered formalin (NBF) at the tissue-volume fixator volume ratio 1:30.

2.3.3. Histological Analysis

The hCPP-samples were explanted with surrounding tissue and assessed, as described below for the subsequent morphological study. Immediately after humane euthanasia, to prevent autolysis instantly after the withdrawal, samples of implanted materials, with surrounding tissues of the recipient bed, were washed for 30 s with a cold (14°C) isotonic solution, and fixed for 48 h in 10% neutral buffered formalin (NBF) at the tissue-volume fixator volume ratio 1:30. For the morphological study, after fixation samples were dehydrated and paraffin embedded. Sections (with a thickness of 4 μm) were prepared and stained using H&E (Mayer's Hematoxylin and Eosin Y) and differential staining for calcium deposits alizarin red S (by the McGee-Russell method and collagen/non-collagen structures (by Lillies trichrome method) [42]. The micrographs of the stained histological samples were obtained on a Nikon Eclipse Ti-E microscope station (Nikon, Tokyo, Japan) and processed using the software NIS Elements AR4.13.05 (Build 933). The maturity of neocollagenous connective tissues around the samples was evaluated with its thickness and a relative area of blood vessels. The high maturity corresponded to minimal inflammation in the low-thickness tissues with a small amount of vessels.

2.4. Statistical Analysis

Results are presented as the mean ± standard deviation (M ± SD). Each of the in vitro experiments was carried out at least four times ($n \geq 4$). The statistical significance of the difference was determined using Mann–Whitney U test. The size of the observed effects was assessed using standardized mean difference (Hedges's g).

The design of the experiment and related statistics (U test) were carried out using Python 3 (ver. 3.10.10) in development environment Spyder (v. 5.4.1) with libraries Pandas (v. 1.5.2), Numpy (v.1.24.2) and Scipy (v. 1.10.0). Plots were created using Python 3 (ver. 3.10.10) with libraries Seaborn (v. 0.12.2) and Matplotlib (v. 3.7.0).

3. Results

3.1. Results of structural and physical-chemical analyses

The hCPPs were obtained by liquid-phase synthesis of HAp by precipitation from solution without subsequent thermal treatment. The synthesis product was a white paste consisting of a fine powder. The results of measurements of the specific surface area of the powders were 80±0.5 m^2/g with the particle size calculated from the specific surface area of hCPP powders being in the range of 25-30 nm. However, the determination of the size of calcium phosphate particles in the region of small sizes is less reliable than the parameter of the coherent scattering region.

Preprints (www.preprints.org) | NOT PEER-REVIEWED | Posted: 18 May 2023 doi:10.20944/preprints202305.1261.v1

Figure 1 shows the IR spectra of both compounds. The precipitate before sintering (Sample-0) has a weak absorption band of the OH- group at 3575 cm^{-1}, indicating low crystallinity of the HA powder. The spectral region from 900 to 1100 cm^{-1} characterizes the symmetric and asymmetric vibrations of the PO_4^{3-} group. The peaks at 564 and 603 cm^{-1} belong to the P-O deformational vibrations (*v4*). The mode at 875 cm^{-1} may belong to both HPO_4^{3-} and CO_3^{2-} groups [43]. The vibrations modes of the CO_3^{2-} group are also detected at 1415 and 1458 cm^{-1}. The peak at 1649 cm^{-1} indicates the presence of adsorbed water. These data are in good agreement with previous studies [44,45].

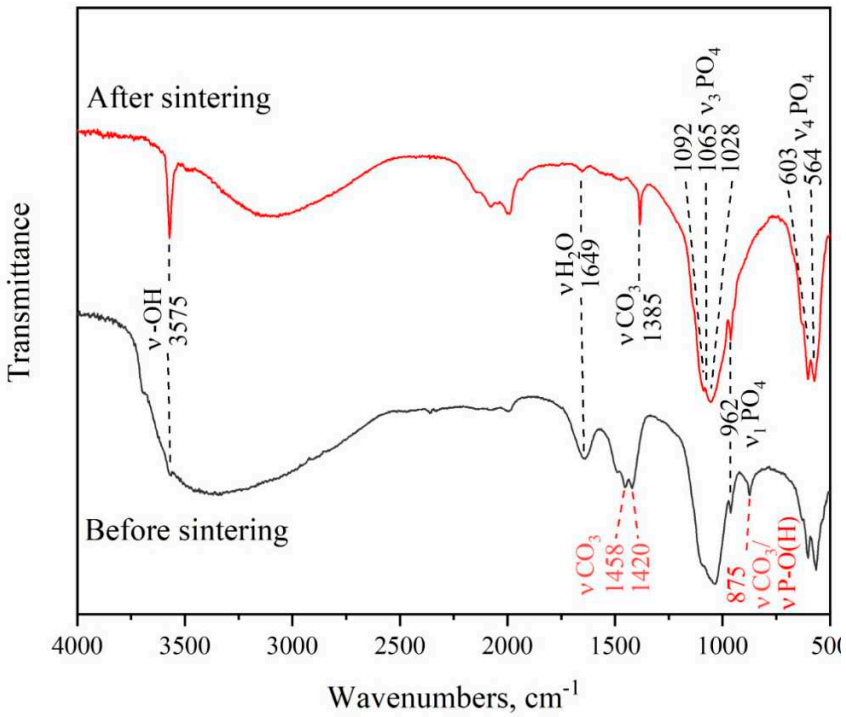

Figure 1. Fourier infrared spectra of hCPP samples after synthesis after firing at 1250 °C.

After sintering, a sharp peak of OH- group appears at 3566 cm^{-1}, indicating an increase in the crystallinity of the samples and the presence of the HAp phase. The peaks of the phosphate groups at 960-1100 cm^{-1} and 550-620 cm^{-1} remain unchanged. The mode of the hydrophosphate group at 875 cm^{-1} decreases. The modes belong to CO_3^{2-} and adsorbed water also decreases.

The results of the X-ray diffraction (XRD) analysis are presented in Figure 2. Before sintering (Sample-0), the precipitate was amorphous (or with a small crystallite size), which causes the FWHM of the nearest peaks to overlap. This leads to difficulties in determining the phase composition and indexing of the diffraction pattern. Some observed maxima on the XRD pattern are a superposition of several peaks. Their indices were compared with card №84-1998 of the XRD base ICDD (Powder Diffraction File, Alphabetical Index Inorganic Compounds, Pensylvania: JCPDS, 1997) and are presented in Table 1. The peaks that are not a superposition of the other two peaks are shifted slightly to the right relative to the card, due to the fact that the diffractogram was taken without a monochromator, that is, the Kα2 shoulder appears at the far angles of 2θ and the peak becomes wider than it actually is. This could lead to not a quite accurate determination of the lattice parameters of the samples. After sintering, the crystallinity of the samples increased, allowing us to identify two phases: HA, corresponding to card №84-1998, and α-TCP, corresponding to card number 29-359. The indices of the reflections of both phases are also presented in Table 1.

Preprints (www.preprints.org) | NOT PEER-REVIEWED | Posted: 18 May 2023 doi:10.20944/preprints202305.1261.v1

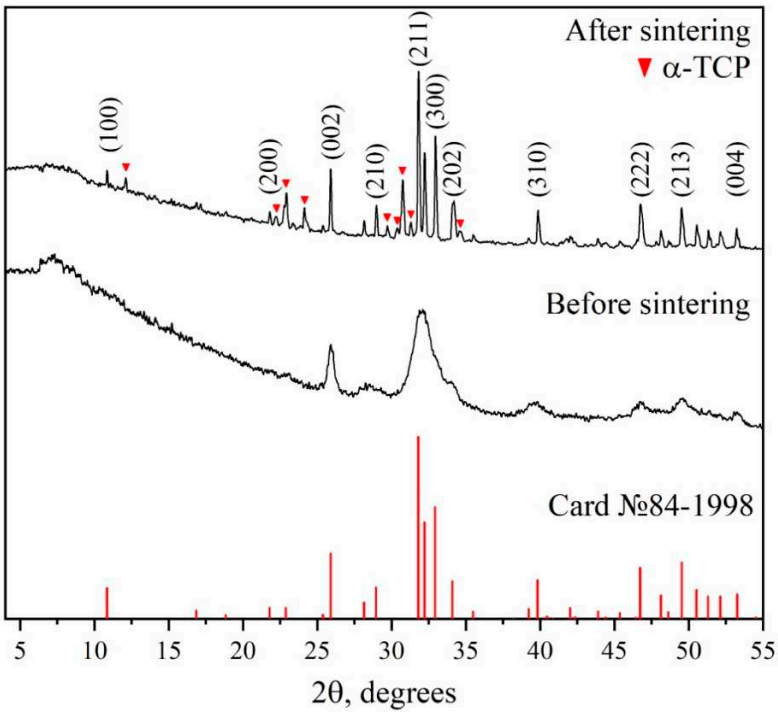

Figure 2. XRD data of hCPP samples upon synthesis after firing at 1250 °C.

Table 1. List of the Peaks Observed in the X-Ray Powder Diffraction Pattern.

Sample-0		HA (1250°C)		HA (1250°C)		α-TCP	
2Theta	(hkl)	2Theta	(hkl)	2Theta	(hkl)	2Theta	(hkl)
		10.86	100	55.98	322	12.11	031
		21.81	200	57.21	313	22.23	201
		22.93	111	58.31	204	22.77	-162
		25.39	201	58.88	330	23.38	-204
25.96	002	25.91	002	60.03	420	23.87	033
28.49	102, 210	28.16	102	60.49	331	24.14	-261
		28.99	210	61.76	421	24.31	043
32.07	211, 112	31.83	211	63.10	502	26.72	-334
		32.24	112	63.53	510	29.73	-361
33.40	300, 202	32.97	300	64.14	304	30.38	-191
		34.17	202	65.18	511	30.76	034
		35.53	301	66.51	422	31.30	-335
39.67	212, 310	39.24	212			34.62	400
		39.88	310			41.43	
		40.48	221			41.76	
		40.87	103				
		42.07	311				
		42.33	302				
		43.90	113				
		44.40	400				
		45.40	203				
46.83	222	46.79	222				
		48.16	312				
		48.71	320				
49.67	213	49.56	213				
		50.59	321				
51.51	410	51.37	410				
		52.17	402				
53.26	004	53.26	004				

The mass ratios in the final product were calculated by the Chang method (corundum numbers). Samples after sintering contain of about 44% of the α-TCP phase. The α-TCP phase is not visible in the IR spectrum because the phosphate groups have the same vibrations as in HA [46]. According to the fact that the HPO_4^{3-} group (mode at 875 cm^{-1}) was present before annealing, we suggested that initially two phases precipitated from the solution: hydroxyapatite $Ca_{10}(PO_4)_6(OH)_2$ and calcium-deficient hydroxyapatite (CDHAp) $Ca_9(HPO_4)(PO_4)_5(OH)$. The diffraction pattern of CDHAp is

Preprints (www.preprints.org) | NOT PEER-REVIEWED | Posted: 18 May 2023 doi:10.20944/preprints202305.1261.v1

presented in card number №46-905. This phase has the same crystal symmetry, space group, and lattice parameters as HA, so it produces reflections that are almost identical to pure HA. However, due to the low crystallinity of our samples, it is not possible to distinguish the phase composition of the precipitate. CDHAp has reflexes with the same Miller indices and at very close angles of two theta as the HA card. The intensity only differs, but not significantly. Upon heating, CDHAp decomposes into α-TCP and water, according to the mechanism described by Y. Li and et al. [47]

$$Ca_9(HPO_4)(PO_4)_5(OH) \rightarrow 3Ca_3(PO_4)_2 + H_2O;$$

Y. Li and co-workers also worked with a biphasic ceramic consisting of α-TCP and HA [48]. The spectra of their intermediate phase are similar to the spectra presented here. The CO_3^{2-} absorption bands at 1415 and 1458 cm^{-1} are also present in the unheated ceramic, but after sintering they merge into a single peak at 1385 cm^{-1}. The authors suggest that the bands at 1415 and 1458 cm^{-1} are characteristic of CO_3^{2-} groups incorporated into the structure of CDHAp [49]. Upon sintering, the CO_3^{2-} group is incorporated into the HA structure, which leads to a slight decrease in lattice parameters (Table 2) [43].

Table 2. The cell dimensions of the natural HA and precipitates formed.

Sample	a(Å)	c(Å)	V(Å3)
Card №84-1998	9.4166	6.8745	527.9
Sample_0	9.39(4)	6.875(12)	525.3(22)
HA	9.4062(18)	6.8707(15)	526.45(15)

3.2. Results of Cytotoxicity Assays

The cytotoxicity of hCPP was studied using mouse mesenchymal cells C3H/10T1/2, based on cell staining with Hoechst 33342 fluorescent dye (stains the nuclei of living and dead cells blue), propidium iodide (stains the nuclei of dead cells red), and calcein AM (stains the cytoplasm of living cells green). All fluorescent dyes were purchased from Sigma–Aldrich (St. Louis, MO, USA). Cells seeded on the culture plastic were used as controls.

When hCPP was added to the C3H/10T1/2 cells for 24 and 96 h, dose-dependent cytotoxicity of the paste-like material was observed (Figure 3). Thus, complete cell death after cultivation with hCPP particles for 24 h was observed only at concentrations of 3 mg/ml or higher. After the first day of cultivation, the number of living cells comparable to the control was observed at a concentration of 0.1 mg/ml (93.60 ± 4.04%). After 96 h of cultivation with hCPP samples, all cells were observed to die at maximum concentrations of 3 mg/ml and 10 mg/ml. At the same time, at standard concentrations of 1.0 and 0.3 mg/ml, a greater number of living cells were observed after 96 h of cultivation, compared with 24 h of cultivation, which indicated the proliferative activity of the cells. Thus, at a concentration of 1 mg/ml after 96h of cultivation, the percentage of living cells increased to 70.67 ±6.02, and at a concentration of 0.3 mg/ml, the value was comparable to that of the control (92.70 ±2.52).

Preprints (www.preprints.org) | NOT PEER-REVIEWED | Posted: 18 May 2023 doi:10.20944/preprints202305.1261.v1

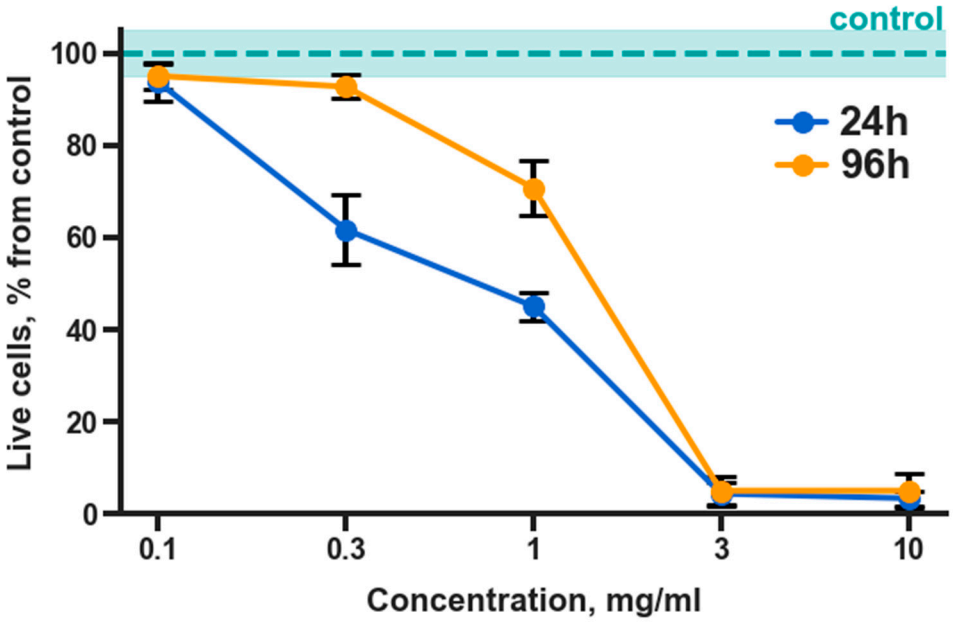

Figure 3. Results of cytotoxic effects of hCPP cultured with Murine embryonic mesenchymal cell line C3H/10T1/2 at concentrations of 0.1, 0.3, 1.0, 3.0, and 10.0 mg/mL, after 24 h and 96 h of cultivation.

Such dose-dependent cytotoxic properties of the material under in vitro conditions may be associated with the presence of an amorphous phase. Since the amorphous phase is characterized by greater solubility than the crystalline one [50], there may be a large release of cytotoxic Ca2+ ions at the cell-material interface due to the acidification of the environment by cells. At the same time, high cell survival in the presence of the studied materials at standard operating concentrations (1.0 mg/ml) and the presence of signs of proliferative activity in the seeded cells indicate the cytocompatibility of the obtained materials. In turn, the presence of an amorphous phase (and free Ca^{2+} ions) in the microenvironment of the material under *in vivo* conditions should have a differentiating effect on progenitor cells during hCPP implantation in the bone environment.

3.3. Results of Protein Adsorption Assay

The first stage of the interaction of a biomaterial with the human body is the sorption of proteins from tissue fluid by its surface. At the same time, with respect to different particles, the key moment of this interaction is the formation of the protein corona surrounding the outer layer of particles [51]. It is believed that the emerging protein corona gives particles a new biological identity, as it changes both physicochemical characteristics and biological properties [52,53]. Therefore, it is important to evaluate the sorption capacity of hCPP. For this purpose, the material was cultured in PBS containing an equivalent amount of protein (10% FBS) in the culture medium for 24 h.

After cultivation of the hCPP with PBS with the addition of 10% FBS, a decrease in the protein content in the incubation medium was observed by 2 times from 3.42±0.16 to 1.64±0.15 mg/ml (Figure 4).

Preprints (www.preprints.org) | NOT PEER-REVIEWED | Posted: 18 May 2023 doi:10.20944/preprints202305.1261.v1

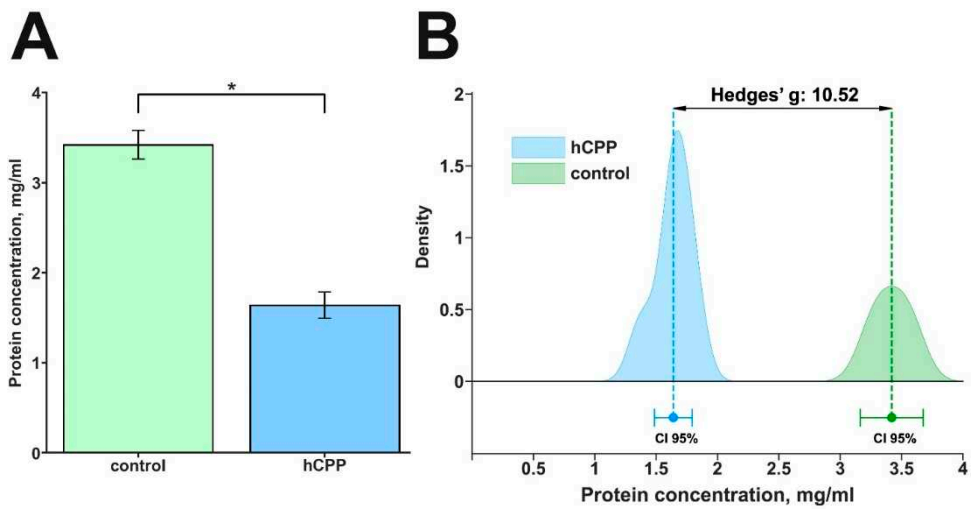

Figure 4. Results of protein adsorption of hCPP (10 mg/ml) cultured with PBS+10% FBS (A). Effect size is shown using the standardized mean difference (Hedges's g). Hedges 's coefficient $g \geq 0.80$ indicates a large effect (B). * – statistically significant difference compared to control, $p<0.05$. CI – confident interval.

These findings (especially the effect size Hedges's g, 10.52) represent the strong sorption capacity of hCPP in relation to proteins.

3.4. Results of in vivo Biocompatibility Assays

Three weeks after subcutaneous injection of hCPP samples into rats, a neocollagen capsule was formed around the material (Figure 5C, yellow dotted line on the capsule-material border) without signs of cell death inside the fibers and fusion of collagen fibers into a dense scar-like fibrous capsule. The neocollagen capsule was saturated with mature microvascular vessels (Figure 5C, black arrows), indicating positive perception of hCPP by the organism. The high maturity of the neocollagenous capsula with a small number of definitive vessels corresponded to minimal inflammation in the surrounding tissues. Simultaneously, the main layer of the material was preserved and represented a sufficiently hydrated calciumphosphate-protein substrate. Inside the capsule, crushing of a solid layer of material by migrating cells into spheres of smaller diameter and their gradual resorption were observed. Resorption of hCPP was performed from the periphery to the center. There were no signs of acute inflammation, as well as signs of material-associated osteogenesis for 3 weeks.

No signs of inflammation or differences from healthy surrounding tissues were observed in the control animals that received an injection of saline solution (Figure 5A,B). After 6 and 13 weeks after injection, the tissues around the injection of the solution were indistinguishable from healthy tissues, as a result of which the histology of these tissues was not further considered.

Preprints (www.preprints.org) | NOT PEER-REVIEWED | Posted: 18 May 2023 doi:10.20944/preprints202305.1261.v1

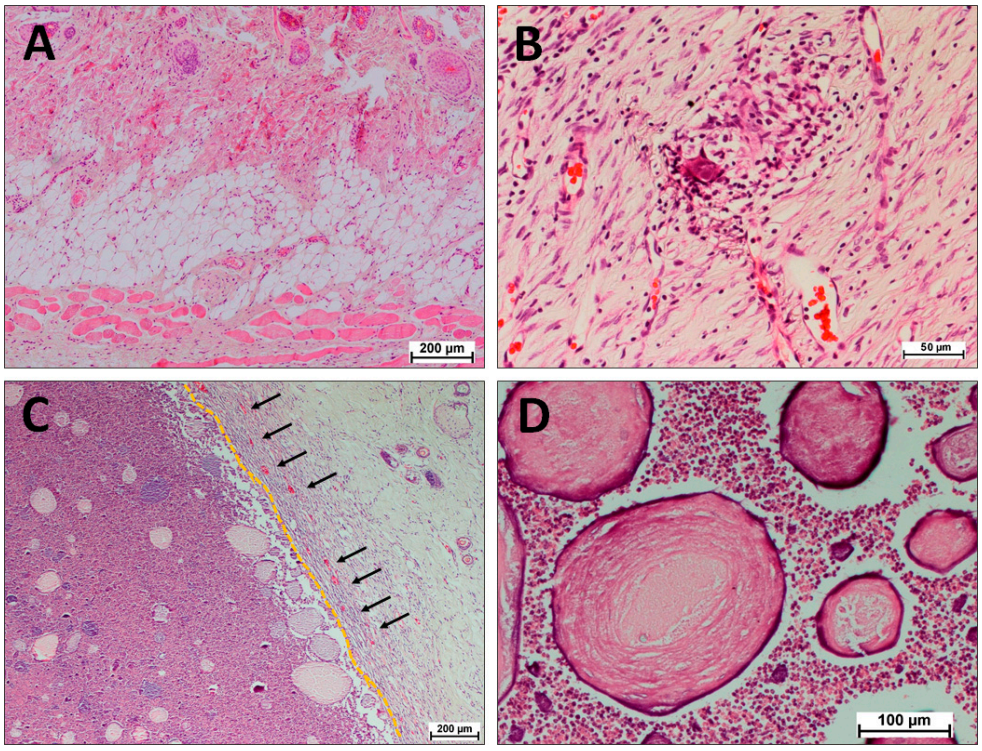

Figure 5. Histological analysis of injected hCPP samples in the control (**A**,**B**) and experimental (**C**,**D**) groups after three weeks. Hematoxylin and eosin staining (H&E, cell nuclei colored blue, erythrocytes colored red, and muscle tissue colored pink); light microscopy. Explanations in the text.

Six weeks after subcutaneous implantation, separation of the capsule material from the hCPP and an increase in the penetration zone of the cells into the material were observed. The hCPP-material lost its hydration at this time and cracked (Figure 6A, B) a relatively loose calciumphosphate-protein substrate with a large number of cells. The capsule around the material was partially calcined, while the calcium deposits were small in size and captured the newly formed collagen tissue around the foci of the hCPP material (Figure 6C). The resorption of hCPP during this observation period averaged at 25%.

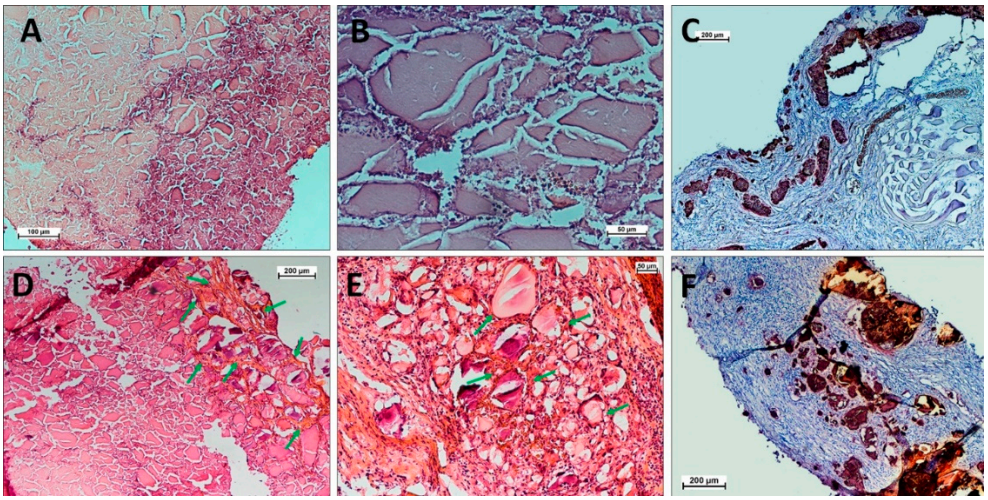

Figure 6. Histological analysis of injected hCPP samples after six (**A**–**C**) and thirteen (**D**–**F**) weeks. (**A**,**B**,**D**,**E**) Hematoxylin and eosin staining (H&E, cell nuclei colored blue, erythrocytes colored red, and muscle tissue colored pink); (**C**,**F**) alizarin red S staining (calcium deposits colored orange-red); light microscopy. Explanations in the text.

Preprints (www.preprints.org) | NOT PEER-REVIEWED | Posted: 18 May 2023 doi:10.20944/preprints202305.1261.v1

Thirteen weeks after subcutaneous injection of hCPP, separation of the material and capsule was observed with pronounced signs of cellular mineralization, which indicated the osteogenic nature of the capsule involution (Figure 6F). At the same time, hCPP-material, as well as for a period of six weeks, was a cracking (Figure 6D,E) relatively loose calciumphosphate-protein substrate with a large number of cells. The resorption of hCPP-material during this observation period averaged at 60%. During this observation period, a distinctive feature of hCPP-material was the formation of a mature collagen matrix around small fragments of hCPP, resembling a spongy extracellular matrix (Figure 6D,E, green arrows).

The results indicated the nontoxicity, biocompatibility, and osteoconductivity of the experimental hCPP, as well as the gradual resorption of hCPP, which was compa-rable to the period of bone regeneration. However, the insufficient osteogenic potential of the studied hCPP demonstrates that it can be successfully used for "fresh" bone trauma, but not in the case of "old" fibrotic trauma or nonunion, which requires mate-rials with additional artificial osteoinductive activity.

Thus, the results obtained by us in the study of injectable hydrated calcium phosphate bone-like paste represent a step towards a new class of minimally invasive, osteoconductive, injectable bone-like pastes with appropriate resorption rates, which are easy to produce and, depending on their physicochemical and biological characteristics, can be carriers of any additional biological activities, thus showing promise for clinical applications in regenerative engineering.

4. Conclusions

Thus, the developed hCPP (under conditions of further modification by selected osteoi- ductive agents) could be a suitable candidate as a safe bone-forming injectable form for bone defect replacement. The study represents a step toward of minimally invasive, osteoconductive, injectable bone-like pastes with appropriate resorption rates, which are easy to produce.

Author Contributions: Conceptualization, I.S.F. and A.Y.T.; methodology, I.V.S. and V.V.M.; validation, R.S.F. and A.S.S.; formal analysis, A.A.A.; investigation, M.I.K.; writing—original draft preparation, V.V.M., A.A.E., P.V.S.; writing—review and editing, I.S.F., A.Y.T. and V.S.K.; visualization, I.V.S.; supervision, V.S.A., and V.S.K. All authors have read and agreed to the published version of the manuscript.

Funding: This research was funded by Russian Science Foundation (RSF, №21-73-20251).

Institutional Review Board Statement: The animal study protocol was approved by the Ethics Committee of Institute of Theoretical and Experimental Biophysics of Russian Academy of Sciences (protocol #26/2022 from 5 March 2022).

Informed Consent Statement: Informed consent was obtained from all subjects involved in the study.

Data Availability Statement: Data available on request from the authors.

Acknowledgments: The work was carried out using the equipment of the Center for the Collective Use of Research Equipment at the ITEB RAS and IMET RAS.

Conflicts of Interest: The authors declare no conflict of interest.

References

1. Raucci MG, D'Amora U, Ronca A, Ambrosio L. Injectable Functional Biomaterials for Minimally Invasive Surgery. *Adv Healthc* Mater. 2020 Jul;9(13):e2000349. doi: 10.1002/adhm.202000349.
2. Subbiah R, Lin EY, Athirasala A, Romanowicz GE, Lin ASP, Califano JV, Guldberg RE, Bertassoni LE. Engineering of an Osteoinductive and Growth Factor-Free Injectable Bone-Like Microgel for Bone Regeneration. *Adv Healthc Mater.* 2023 Apr;12(11):e2200976. doi: 10.1002/adhm.202200976.
3. Phogat K., Ghosh S.B., Bandyopadhyay-Ghosh S. Recent advances on injectable nanocomposite hydrogels towards bone tissue rehabilitation. *J Appl Polymer Sci*. 2023; 140(4): e53362. doi: 10.1002/app.53362
4. Harrison CJ, Hatton PV, Gentile P, Miller CA. Nanoscale Strontium-Substituted Hydroxyapatite Pastes and Gels for Bone Tissue Regeneration. *Nanomaterials (Basel).* 2021 Jun 19;11(6):1611. doi: 10.3390/nano11061611.

Preprints (www.preprints.org) | NOT PEER-REVIEWED | Posted: 18 May 2023 doi:10.20944/preprints202305.1261.v1

5. Zeimaran E, Pourshahrestani S, Fathi A, Razak NABA, Kadri NA, Sheikhi A, Baino F. Advances in bioactive glass-containing injectable hydrogel biomaterials for tissue regeneration. *Acta Biomater*. 2021 Dec;136:1-36. doi: 10.1016/j.actbio.2021.09.034.
6. Hao J, Chou J, Kuroda S, Otsuka M, Kasugai S, Lang NP. Strontium hydroxyapatite in situ gel-forming system - a new approach for minimally invasive bone augmentation. *Clin Oral Implants Res.* 2015 May;26(5):581-5. doi: 10.1111/clr.12446.
7. Qu Y, Zhuang H, Zhang M, Wang Y, Zhai D, Ma B, Wang X, Qin C, Huan Z, Wu C. Bone cements for therapy and regeneration for minimally invasive treatment of neoplastic bone defects. *J Mater Chem B.* 2021 Jun 3;9(21):4355-4364. doi: 10.1039/d1tb00703c.
8. Fortune Business Insights Available online: https://www.researchandmarkets.com/reports/5206327/bone-grafts-and-substitutes-market-by-type
9. O'Neill R, McCarthy HO, Montufar EB, Ginebra MP, Wilson DI, Lennon A, Dunne N. Critical review: Injectability of calcium phosphate pastes and cements. *Acta Biomater*. 2017 Mar 1;50:1-19. doi: 10.1016/j.actbio.2016.11.019.
10. Xu HH, Wang P, Wang L, Bao C, Chen Q, Weir MD, Chow LC, Zhao L, Zhou X, Reynolds MA. Calcium phosphate cements for bone engineering and their biological properties. *Bone Res.* 2017 Dec 20;5:17056. doi: 10.1038/boneres.2017.56.
11. Yasmeen S, Lo MK, Bajracharya S, Roldo M. Injectable scaffolds for bone regeneration. *Langmuir.* 2014 Nov 4;30(43):12977-85. doi: 10.1021/la503057w.
12. Bai X, Gao M, Syed S, Zhuang J, Xu X, Zhang XQ. Bioactive hydrogels for bone regeneration. *Bioact Mater.* 2018 May 26;3(4):401-417. doi: 10.1016/j.bioactmat.2018.05.006.
13. Fang, CH., Lin, YW., Sun, JS. et al. The chitosan/tri-calcium phosphate bio-composite bone cement promotes better osteo-integration: an in vitro and in vivo study. *J Orthop Surg Res* 14, 162 (2019). https://doi.org/10.1186/s13018-019-1201-2
14. Khandaker M, Meng Z. The Effect of Nanoparticles and Alternative Monomer on the Exothermic Temperature of PMMA Bone Cement. *Procedia Eng*. 2015;105:946-952. doi: 10.1016/j.proeng.2015.05.120.
15. Khandaker M, Vaughan MB, Morris TL, White JJ, Meng Z. Effect of additive particles on mechanical, thermal, and cell functioning properties of poly(methyl methacrylate) cement. *Int J Nanomed*. 2014;9:2699–712.
16. Jeong, J., Kim, J.H., Shim, J.H. et al. Bioactive calcium phosphate materials and applications in bone regeneration. *Biomater Res* 23, 4 (2019). https://doi.org/10.1186/s40824-018-0149-3
17. Alt V, Bechert T, Steinrucke P, Wagener M, Seidel P, Dingeldein E, Domann E, Schnettler R. An in vitro assessment of the antibacterial properties and cytotoxicity of nanoparticulate silver bone cement. *Biomaterials.* 2004;25-18:4383–4391.
18. Lodoso-Torrecilla I, van den Beucken JJJP, Jansen JA. Calcium phosphate cements: Optimization toward biodegradability. *Acta Biomater.* 1 Jan 2021;119:1-12. doi: 10.1016 /j.actbio.2020.10.013.
19. Liu S, Fu H, Lv Y, Jiao J, Guo R, Yang Y, Dong W, Mi H, Wang M, Liu M, Li R. α-Hemihydrate calcium sulfate/n-hydroxyapatite combined with metformin promotes osteogenesis in vitro and in vivo. *Front Bioeng Biotechnol*. 2022 Sep 30;10:899157. doi: 10.3389/fbioe.2022.899157.
20. Nauth A, Lane J, Watson JT, Giannoudis P. Bone Graft Substitution and Augmentation. *J Orthop Trauma.* 2015 Dec;29 Suppl 12:S34-8. doi: 10.1097/BOT.0000000000000464.
21. Portnov, T., Shulimzon, T. & Zilberman, M. (2017). Injectable hydrogel-based scaffolds for tissue engineering applications. *Reviews in Chemical Engineering*, 33(1), 91-107. https://doi.org/10.1515/revce-2015-0074
22. Perez RA, Kim HW, Ginebra MP. Polymeric additives to enhance the functional properties of calcium phosphate cements. *J Tissue Eng.* 2012;3(1):2041731412439555. doi: 10.1177/2041731412439555.
23. Moreira CDF, Carvalho SM, Florentino RM, França A, Okano BS, Rezende CMF, Mansur HS, Pereira MM. Injectable chitosan/gelatin/bioactive glass nanocomposite hydrogels for potential bone regeneration: In vitro and in vivo analyses. *Int J Biol* Macromol. 2019 Jul 1;132:811-821. doi: 10.1016/j.ijbiomac.2019.03.237.
24. Kantak MN, Bharate SS. Analysis of clinical trials on biomaterial and therapeutic applications of chitosan: A review. *Carbohydr Polym.* 2022 Feb 15;278:118999. doi: 10.1016/j.carbpol.2021.118999.
25. Kean T, Thanou M. Biodegradation, biodistribution and toxicity of chitosan. *Adv Drug Deliv Rev.* 2010 Jan 31;62(1):3-11. doi: 10.1016/j.addr.2009.09.004.

Preprints (www.preprints.org) | NOT PEER-REVIEWED | Posted: 18 May 2023 doi:10.20944/preprints202305.1261.v1

26. Masson JD, Thibaudon M, Bélec L, Crépeaux G. Calcium phosphate: a substitute for aluminum adjuvants? *Expert Rev Vaccines.* 2017 Mar;16(3):289-299. doi: 10.1080/14760584.2017.1244484.
27. Lin Y, Wang X, Huang X, Zhang J, Xia N, Zhao Q. Calcium phosphate nanoparticles as a new generation vaccine adjuvant. *Expert Rev Vaccines*. 2017 Sep;16(9):895-906. doi: 10.1080/14760584.2017.1355733.
28. Niculescu AG, Grumezescu AM. Applications of Chitosan-Alginate-Based Nanoparticles-An Up-to-Date Review. *Nanomaterials (Basel).* 2022 Jan 6;12(2):186. doi: 10.3390/nano12020186.
29. Wack A, Baudner BC, Hilbert AK, Manini I, Nuti S, Tavarini S, Scheffczik H, Ugozzoli M, Singh M, Kazzaz J, Montomoli E, Del Giudice G, Rappuoli R, O'Hagan DT. Combination adjuvants for the induction of potent, long-lasting antibody and T-cell responses to influenza vaccine in mice. *Vaccine*. 2008 Jan 24;26(4):552-61. doi: 10.1016/j.vaccine.2007.11.054.
30. Mallakpour S, Azadi E, Hussain CM. Chitosan, alginate, hyaluronic acid, gums, and β-glucan as potent adjuvants and vaccine delivery systems for viral threats including SARS-CoV-2: A review. *Int J Biol Macromol*. 2021 Jul 1;182:1931-1940. doi: 10.1016/j.ijbiomac.2021.05.155.
31. Hruschka V., Tangl S., Ryabenkova Y., Heimel P., Barnewitz D., Mobus G., Keibl C., Ferguson J., Quadros P., Miller C., et al. Comparison of nanoparticular hydroxyapatite pastes of different particle content and size in a novel scapula defect model. *Sci. Rep.* 2017;7:43425. doi: 10.1038/srep43425.
32. Fox K., Tran P.A., Tran N. Recent advances in research applications of nanophase hydroxyapatite. *Chemphyschem.* 2012;13:2495–2506. doi: 10.1002/cphc.201200080.
33. Liu Z, Yamada S, Otsuka Y, Peñaflor Galindo TG, Tagaya M. Surface modification of hydroxyapatite nanoparticles for bone regeneration by controlling their surface hydration and protein adsorption states. *Dalton Trans.* 2022 Jun 27;51(25):9572-9583. doi: 10.1039/d2dt00969b.
34. Masouleh, M.P.; Hosseini, V.; Pourhaghgouy, M.; Bakht, M. Calcium Phosphate Nanoparticles Cytocompatibility Versus Cytotoxicity: A Serendipitous Paradox. *Curr. Pharm. Des*. 2017, 23, 2930–2951.
35. Velard, F.; Braux, J.; Amedee, J.; Laquerriere, P. Inflammatory cell response to calcium phosphate biomaterial particles: An overview. *Acta Biomater*. 2013, 9, 4956–4963.
36. Mulay, S.R.; Anders, H.-J. Crystallopathies. *N. Engl. J. Med*. 2016, 374, 2465–2476.
37. Chen, Y.; Liu, Z.; Jiang, T.; Zou, X.; Lei, L.; Yan, W.; Yang, J.; Li, B. Strontium-Substituted Biphasic Calcium Phosphate Microspheres Promoted Degradation Performance and Enhanced Bone Regeneration. *J Biomed Mater Res A* 2020, 108, 895–905, doi:10.1002/jbm.a.36867.
38. Bradford, M.M. A Rapid and Sensitive Method for the Quantitation of Microgram Quantities of Protein Utilizing the Principle of Protein-Dye Binding. *Anal Biochem* 1976, 72, 248–254, doi:10.1006/abio.1976.9999.
39. Barradas, A.M.; Yuan, H.; van Blitterswijk, C.A.; Habibovic, P. Osteoinductive biomaterials: Current knowledge of properties, experimental models and biological mechanisms. *Eur. Cell Mater* 2011, 21, 407–429; discussion 429.
40. Fadeeva, I.S.; Teterina, A.Y.; Minaychev, V.V.; Senotov, A.S.; Smirnov, I.V.; Fadeev, R.S.; Smirnova, P.V.; Menukhov, V.O.; Lomovskaya, Y.V.; Akatov, V.S.; Barinov, S.M.; Komlev, V.S. Biomimetic Remineralized Three-Dimensional Collagen Bone Matrices with an Enhanced Osteostimulating Effect. *Biomimetics* 2023, 8, 91. https://doi.org/10.3390/biomimetics8010091
41. Lillie, R.D.; Fullmer, H.M. Histopathologic Technic and Practical Histochemistry—Front Cover; McGraw-Hill: San Francisco, CA, USA, 1976; p. 942.
42. Van der Houwen J. A. M. et al. The effect of organic ligands on the crystallinity of calcium phosphate. *Journal of Crystal Growth.* 2003. Т. 249. №. 3-4. p. 572-583.
43. Koutsopoulos S. Synthesis and characterization of hydroxyapatite crystals: a review study on the analytical methods //Journal of Biomedical Materials Research: An Official Journal of the Society for Biomaterials, The Japanese Society for Biomaterials, and The Australian Society for Biomaterials and the Korean Society for Biomaterials. 2002. Т. 62. №. 4. p. 600-612.
44. Jemli Y. E. L. et al. Synthesis and Characterization of Hydroxyapatite and Hydroxyapatite-Based Catalysts. Design and Applications of Hydroxyapatite-Based Catalysts. 2022. p. 19-72.
45. Kolmas J. et al. Alpha-tricalcium phosphate synthesized by two different routes: Structural and spectroscopic characterization. *Ceramics international*. 2015. Т. 41. №. 4. p. 5727-5733
46. Yubao L., Xingdong Z., De Groot K. Hydrolysis and phase transition of alpha-tricalcium phosphate. *Biomaterials*. 1997. Т. 18. №. 10. p. 737-741.
47. Li Y., Kong F., Weng W. Preparation and characterization of novel biphasic calcium phosphate powders (α-TCP/HA) derived from carbonated amorphous calcium phosphates. *Journal of Biomedical Materials*

Preprints (www.preprints.org) | NOT PEER-REVIEWED | Posted: 18 May 2023 doi:10.20944/preprints202305.1261.v1

Research Part B: Applied Biomaterials: An Official Journal of The Society for Biomaterials, The Japanese Society for Biomaterials, and The Australian Society for Biomaterials and the Korean Society for Biomaterials. 2009. Т. 89. №. 2. p. 508-517

48. Falk M., Miller A. G. Infrared spectrum of carbon dioxide in aqueous solution. *Vibrational spectroscopy*. 1992. Т. 4. №. 1. p. 105-108.
49. Rey, C.; Combes, C.; Drouet, C.; Grossin, D.; Bertrand, G.; Soulié, J. 1.11 Bioactive Calcium Phosphate Compounds: Physical Chemistry. In Comprehensive Biomaterials II; Ducheyne, P., Ed.; Elsevier: Oxford, 2017; pp. 244–290 ISBN 978-0-08-100692-4.
50. Rampado, R.; Crotti, S.; Caliceti, P.; Pucciarelli, S.; Agostini, M. Recent Advances in Understanding the Protein Corona of Nanoparticles and in the Formulation of "Stealthy" Nanomaterials. Frontiers in Bioengineering and Biotechnology 2020, 8.
51. Bai, X.; Wang, J.; Mu, Q.; Su, G. In Vivo Protein Corona Formation: Characterizations, Effects on Engineered Nanoparticles' Biobehaviors, and Applications. Frontiers in Bioengineering and Biotechnology 2021, 9.
52. Miclăuş, T.; Beer, C.; Chevallier, J.; Scavenius, C.; Bochenkov, V.E.; Enghild, J.J.; Sutherland, D.S. Dynamic Protein Coronas Revealed as a Modulator of Silver Nanoparticle Sulphidation in Vitro. *Nat Commun* 2016, 7, 11770, doi:10.1038/ncomms11770.

Disclaimer/Publisher's Note: The statements, opinions and data contained in all publications are solely those of the individual author(s) and contributor(s) and not of MDPI and/or the editor(s). MDPI and/or the editor(s) disclaim responsibility for any injury to people or property resulting from any ideas, methods, instructions or products referred to in the content.